SUPPLEMENTARY INFORMATION

Raman Spectroscopy of Electrochemically Exfoliated Graphene: Defect Evolution, Doping Effects, and Interpretive Frameworks

M.J Madito

Institute for Nanotechnology and Water Sustainability (iNanoWS), College of Science, Engineering and Technology,

University of South Africa, Johannesburg 1710, South Africa

Raman Scattering Processes in Graphene

At the *Γ* point, phonon modes correspond to the irreducible representations of the crystal's symmetry group. In pristine (defect-free, and undoped) monolayer graphene (1LG), the unit cell contains two carbon atoms, giving rise to six vibrational modes at the *Γ* point (**Figure S1**): three acoustic branches (the in-plane longitudinal acoustic (LA), transverse acoustic (TA), and out-of-plane acoustic (ZA), and three optical branches (longitudinal optical (LO), transverse optical (TO), and out-of-plane optical (ZO)) [1,2]. These include the doubly degenerate in-plane E_{2g} mode (Raman-active) and the out-of-plane B_{2g} mode (inactive). Graphite, with four atoms per unit cell, displays twelve modes due to interlayer coupling but retains the same D_{6h} symmetry as 1LG. The acoustic modes in both materials comprise A_{2u} and E_{1u} symmetries, while the optical modes are split in graphite due to Davydov splitting [1–3]. The most prominent Raman-active band in both graphene and graphite is the G band (≈1582 cm^{-1}, **Figure S1**), originating from the E_{2g} mode at the *Γ* point and corresponding to bond stretching of sp^2 carbon atoms [4–6].

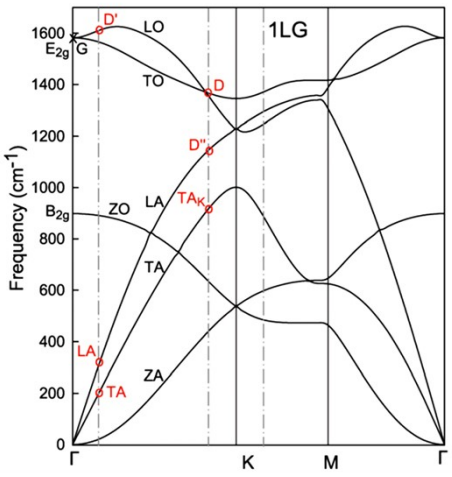

Figure S1. *Phonon dispersion curves of 1LG calculated by density functional perturbation theory. Reproduced with permission from Ref. [7]. Copyright 2008, American Physical Society.*

Moreover, **Figure S2** illustrates the primary Raman scattering processes in pristine 1LG. According to the Raman selection rule of momentum conservation, only phonons near the Brillouin zone center (*Γ* point) can be Raman active in a first-order process, provided they are symmetry-allowed [3]. The G band, arising from such a first-order process, is the only mode allowed at the *Γ* point and involves in-plane optical phonons with E_{2g} symmetry (**Figure S2(a)**). In 1LG, where linear electronic bands intersect at the Dirac point, an incident photon with energy ε_L can resonantly excite an electron from the valence band (state *a*) to the conduction band (state *b*). The excited electron can be scattered by the E_{2g} phonons to recombine with a hole, satisfying either an incoming or outgoing resonance condition. Other prominent Raman bands in graphene (**Figure S2(b-g)**) arise from double- or triple-resonance (DR or TR) processes that involve one or two phonons with finite momentum and, in some cases, a defect [1–3]. One-phonon DR processes require a defect to satisfy momentum conservation, thus activating otherwise forbidden modes. The D′ (≈1620 cm^{-1}) and 2D′ (≈3240 cm^{-1}) bands originate from intravalley DR processes, involving one or two longitudinal optical (LO) phonons near the *Γ* point, respectively **(Figure S2(b,c)** and **Figure S1**) [8]. The D′ band requires a defect, while the 2D′ band is activated via two-phonon processes and does not require defects.

The D and 2D bands result from intervalley DR processes involving transitions between nonequivalent Dirac cones (*K* and *K′*) (**Figure S2(d,e)**). The D band (≈1350 cm^{-1}) arises from a one-phonon DR process where a TO phonon near the *K* (or *K′*) point is activated by a defect. At this point, an electron excited by ε_L is scattered first by a phonon and then by a defect (or vice versa) before recombination (**Figure S2(d)**). In contrast, the 2D band (≈2700 cm^{-1}) arises from a defect-free two-phonon DR process involving back-to-back scattering of the photoexcited electron and hole by two TO phonons with opposite momenta (±q), enabled by the near mirror symmetry of the conduction and valence bands (**Figure S2(e)**). Both the excitation and recombination steps are resonant, resulting in the high intensity of the 2D band [9,10]. The dominant phonon contributions to both the D and 2D bands are from those along the *Γ*-*K* direction [11]. Additionally, an LA phonon near the *K* point can be activated by a defect in an intervalley DR process, leading to the D″ band at ≈1150 cm^{-1}.

Figure S2 primarily illustrates inner intervalley DR and TR processes that activate phonons along the *Γ*-*K* direction. However, outer processes (**Figure S2(f,g)**), involving phonons along the *K*-*M* direction, can also satisfy the DR/TR conditions. For each excitation energy ε_L, different phonon branches (as shown in **Figure S1**) may contribute to intravalley or intervalley Raman processes. Nevertheless, due to variation in electron-phonon coupling strengths, not all phonons excited by ε_L are observed in the Raman spectra.

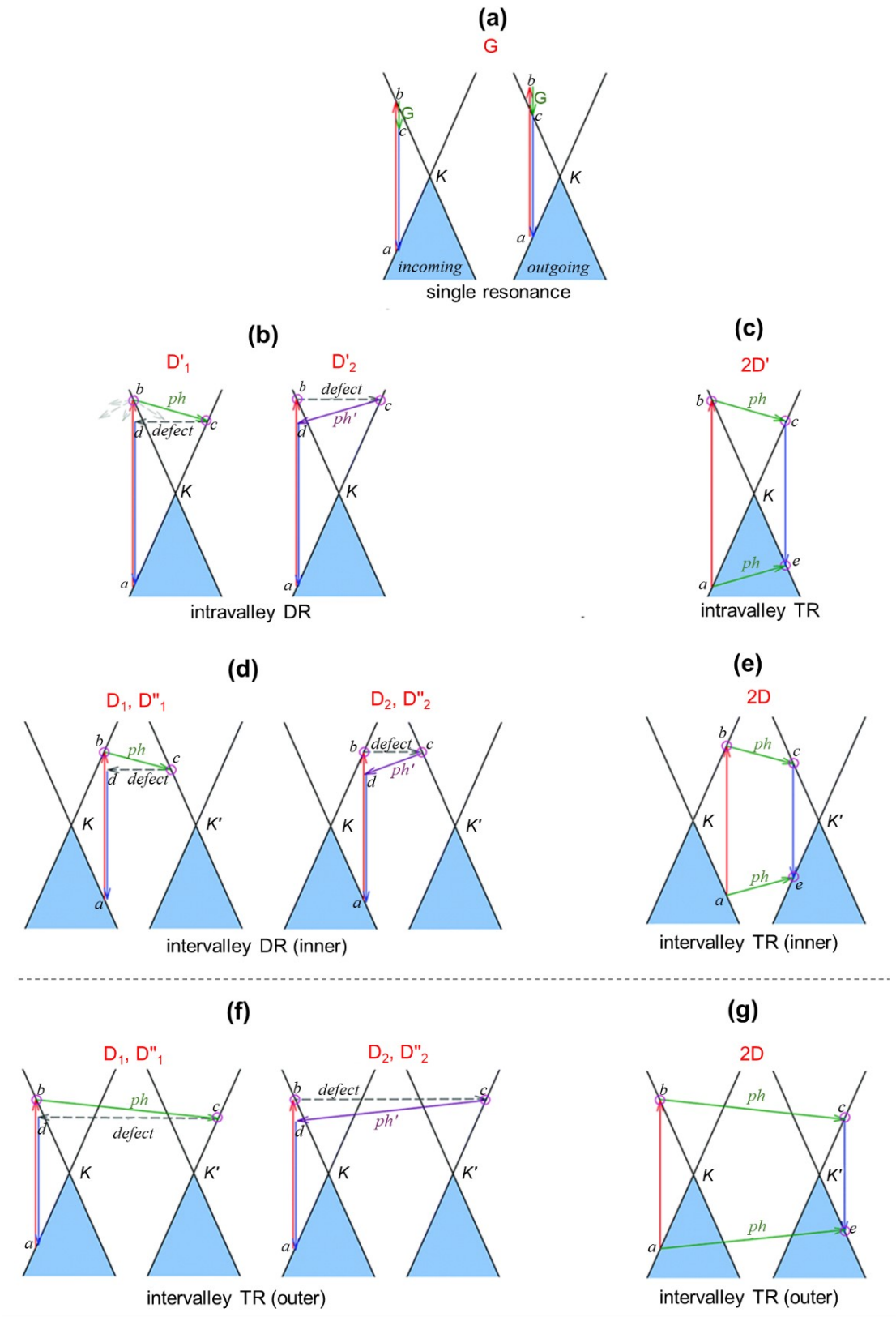

Figure S2. *Raman processes in 1LG: (a) Incoming and outgoing single resonance processes of the G mode. (b-e) Resonant processes of dispersive Raman modes in 1LG, including an electron-hole pair excited by an incident laser photon, inelastic scattering of the electron and hole by phonon emission/absorption, and elastic scattering of the electron mediated by the defect, and recombination of the electron-hole pair. (b) The intravalley double resonance processes. (c) An intravalley triple*

resonance process. (d,e) The inner intervalley double and triple resonance processes. (f,g) The outer intervalley double and triple resonance processes. Reproduced with permission from Ref. [22]. Copyright 2018, The Royal Society of Chemistry.

Raman spectrum of electrochemically exfoliated graphene

The Raman spectrum of EEG typically exhibits prominent D (≈1343 cm^{-1}), G (≈1580 cm^{-1}), and 2D (≈2700 cm^{-1}) bands (**Figure S3**), along with additional defect-related features such as the D′ (≈1615 cm^{-1}) and D″ (≈1140 cm^{-1}) bands. The D band is often significantly intensified in EEG as a result of chemical heterogeneity arising from electrochemical exfoliation, including the incorporation of oxygen-containing functional groups and the coexistence of sp^2- and sp^3-hybridized carbon domains. These chemical modifications contribute to increased structural disorder, which enhances defect-mediated Raman scattering processes and gives rise to additional disorder-related spectral features. In addition to the characteristic D and G bands, some EEG samples exhibit a weak, broad Raman feature in the 1450 - 1550 cm^{-1} range (1530 cm^{-1} band, **Figure S3**, denoted as D_2″). While this intermediate band is not assigned to a well-defined phonon mode in pristine 1LG, it is likely activated through disorder-induced scattering involving LA or mixed phonon branches along the *Γ-K* direction. Its appearance is often attributed to structural disorder, edge defects, or vibrational modes associated with oxygen-containing functional groups. A similar feature has been reported in disordered carbon materials and is frequently linked to amorphous carbon contributions or localized vibrational states arising from chemical heterogeneity [12].

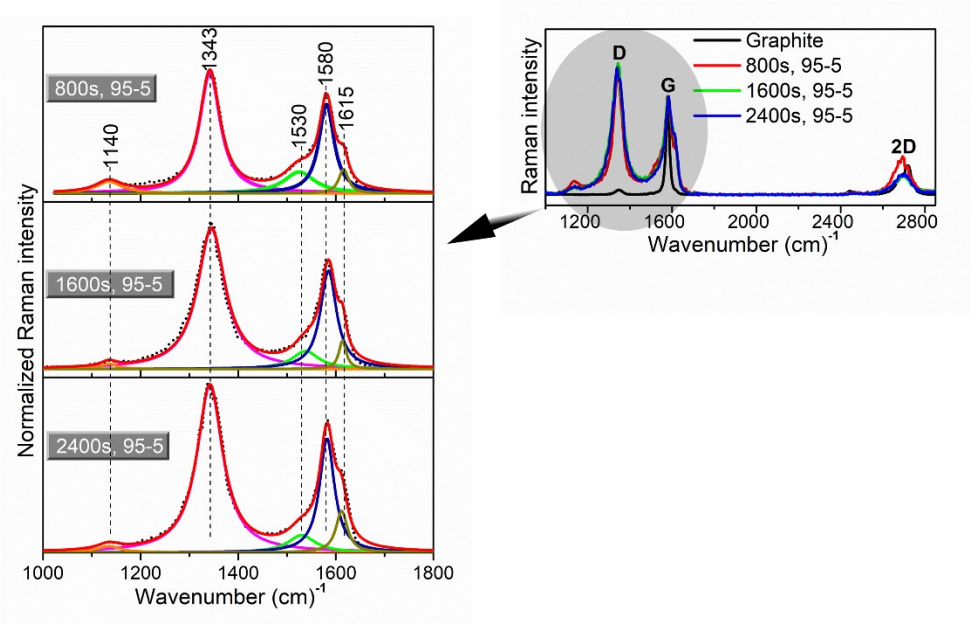

Figure S3. *Raman spectra of graphite foil and EEG intercalated from 800 to 2400 s in 95-5, 90-10, and 80-20 H_2SO_4 to H_3PO_4 acid blends, and the corresponding Lorentzian fitting (solid lines). Reproduced with permission from Ref. [13]. Copyright 2020, Elsevier Ltd.*

Table S1 summarizes previously published studies on electrochemically exfoliated few-layer graphene, detailing the electrolytes and processing conditions employed, along with the resulting flake morphology, defect density, Raman features, and X-ray diffraction (XRD) characteristics. Based on these reports, the Raman parameters discussed in this review, namely the I(D)/I(G) ratio, G-band position, G-band full width at half maximum (FWHM), 2D-band position, 2D-band FWHM, and I(D′)/I(G) ratio, were extracted from the Raman spectra compiled in **Table S1**. All Raman measurements were performed using a 523 nm excitation laser.

Table S1. *Summary of reported studies on electrochemically exfoliated few-layer graphene (<10 layers), including exfoliation electrolytes, key process parameters, resulting sheet morphology (flake size, thickness, and defect density), characteristic Raman features (D, G, and 2D band positions and intensity ratios), and typical XRD patterns observed under varying experimental conditions.*

Exfoliation electrolyte, and parameters	**Morphology**	**Corresponding Raman spectra**	**Corresponding XRD patterns**	**Ref.**
0.1 M $(NH_4)_2S_2O_8$; +12 V DC; complete exfoliation	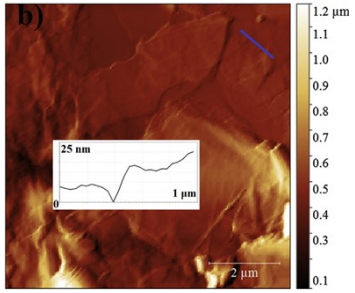 Wrinkled few-layer graphene sheets (5 nm thick)	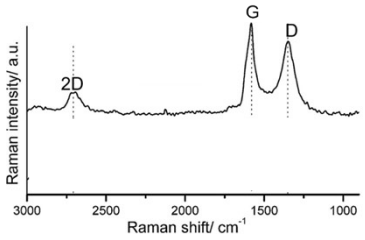 Laser source = 532 nm	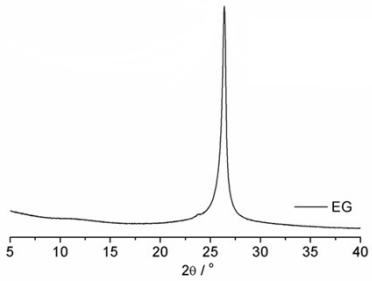 *Reproduced with permission from Ref. [14], Copyright 2016, Elsevier Ltd.*	14
0.05-1 M $(NH_4)_2HPO_4$; +10 V DC; complete exfoliation *$(NH_4)_2HPO_4$ minimizes oxidation	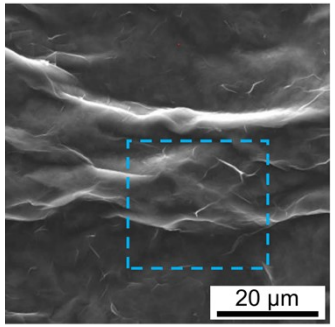	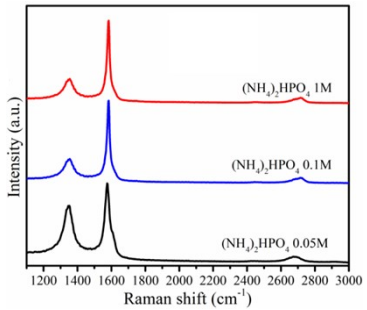	No XRD reported	15

	Few-layer graphene sheets (1-4 layers) C/O ratio ≈ 4	Laser source = 532 nm *Reproduced with permission from Ref. [15], Copyright 2019, Elsevier Ltd.*		
0.1 M $NH_4(SO_4)$; +10 V DC; 1600 s	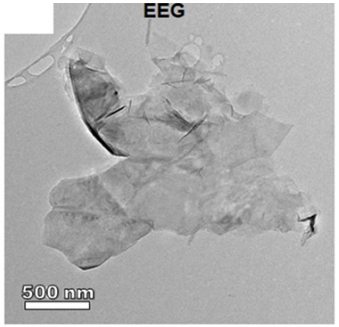 Few-layer graphene sheets; C/O ratio = 4	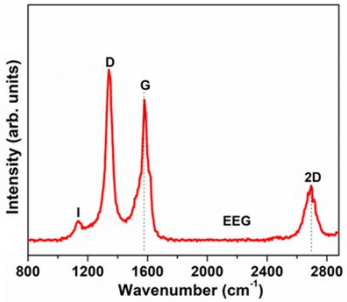 Laser source = 532 nm	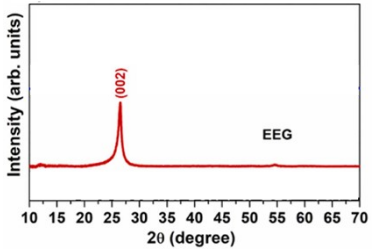 *Reproduced with permission from Ref. [16], Copyright 2024, Elsevier B.V.*	16
0.1 M $(NH_4)_2(SO_4)$; +10 V DC; 60 s	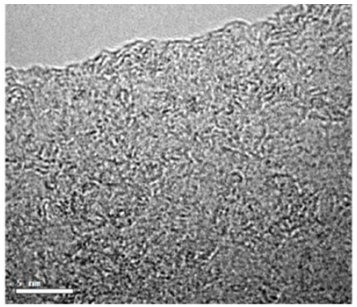 Multilayer graphene sheets (1-3 layers); C/O ratio = 17.2	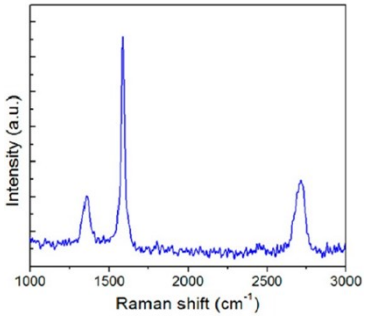 Laser source = 532 nm	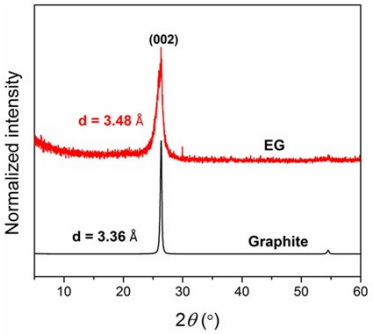 *Reproduced with permission from Ref. [17], Copyright 2014, American Chemical Society*	17

0.1 M $(NH_4)_2SO_4$ + (2,2,6,6,tetramethyl-piperidinyl) oxyl (TEMPO); +10 V DC; 10 s	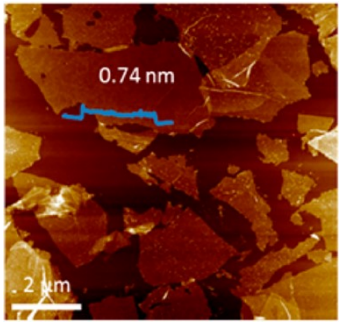 Few-layer graphene flakes, 5-10 µm on average (1-3 layers); C/O ratio = 25.3	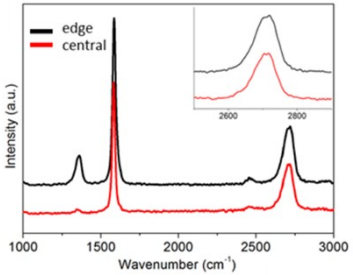 Laser source = 532 nm *Reproduced with permission from Ref. [18], Copyright 2015, American Chemical Society*	No reported XRD	18
Tetra-n-butylammonium bisulphate ($TBA{\cdot}HSO_4$) aqueous solution (0.1 M, pH 1.8) ±10 V AC (0.1 Hz); 20 g/h	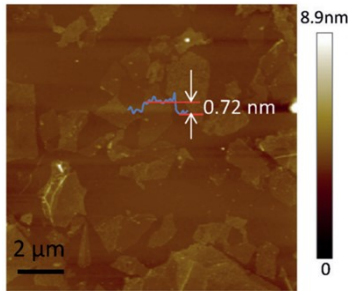 Few-layer graphene flakes, 1-5 µm on average (1-4 layers); C/O ratio = 21.2	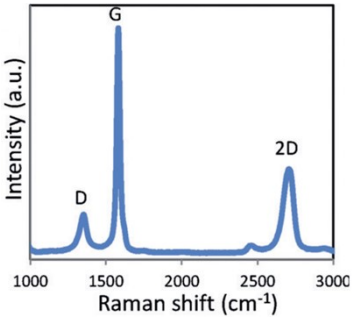 Laser source = 532 nm *Reproduced with permission from Ref. [19], Copyright 2017, Wiley-VCH Verlag GmbH & Co. KGaA, Weinheim*	No reported XRD	19

0.1 H_2SO_4 +1 mg.ml^{-1} melamine; ±20 V DC; 10 min	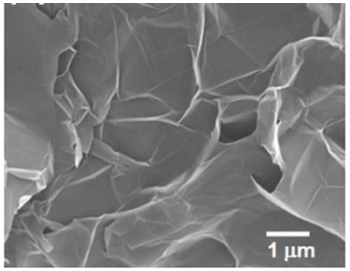 Wrinkled few-layer graphene sheets (1-4 layers); C/O ratio = 26.17	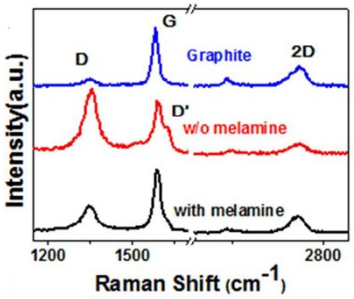 Laser source = 532 nm	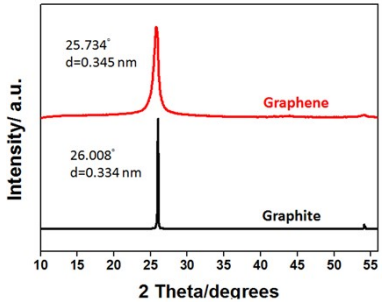 *Reproduced with permission from Ref. [20], Copyright 2015, The Royal Society of Chemistry*	20
0.1 M $(NH_4)_2SO_4$; +10 V DC; 6 h	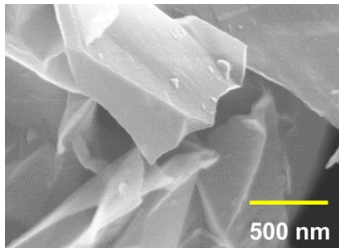 Wrinkled multilayer graphene sheets; C/O ratio = 6.13	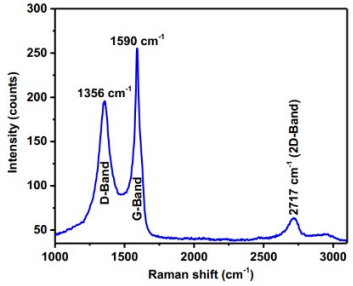 Laser source = 532 nm	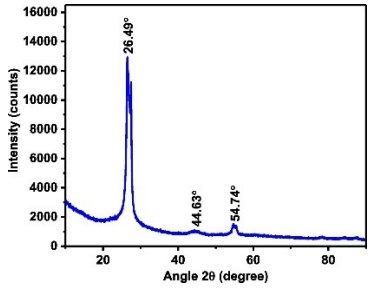 *Reproduced with permission from Ref. [21], Copyright 2021, Elsevier B.V.*	21

0.1 M $(NH_4)_2SO_4$; +10 V DC; 4 h	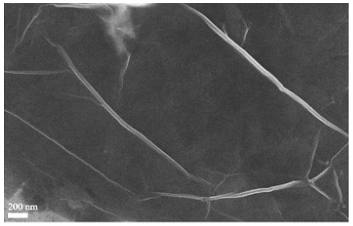 Wrinkled multilayer graphene sheets; C/O ratio = 4.58	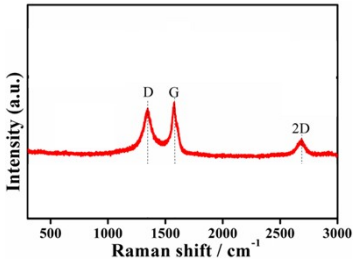 Laser source = 532 nm	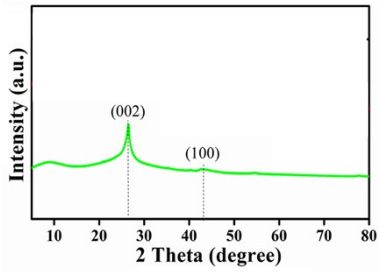 *Reproduced with permission from Ref. [22], Copyright 2016, Springer-Verlag Berlin Heidelberg.*	22
0.1 M Na_2SO_4; +10 V DC; 60 min	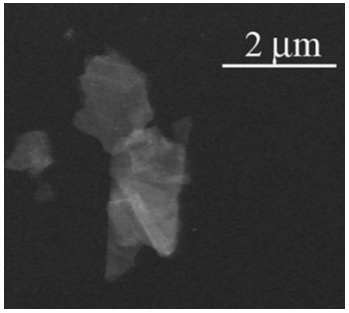 Wrinkled multilayer graphene sheets (2 nm thick); C/O ratio = 9.09	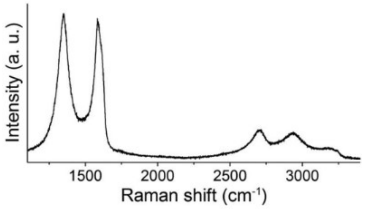 Laser source = 532 nm *Reproduced with permission from Ref. [23], Copyright 2016, The Royal Society of Chemistry*	No reported XRD	23

0.1 M $(NH_4)_2SO_4$; +10 V DC; several minutes	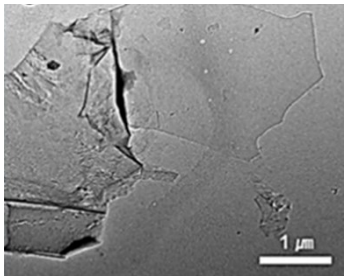 Wrinkled multilayer graphene sheets (2-5 layers); C/O ratio = 14.9	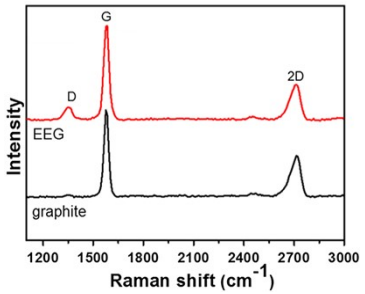 Laser source = 532 nm	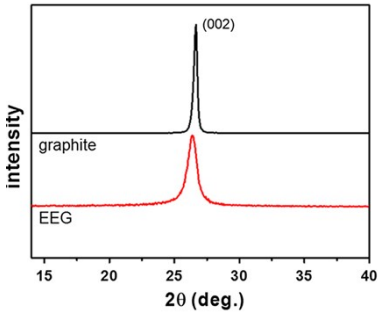 *Reproduced with permission from Ref. [24], Copyright 2019, Korean Carbon Society*	24
0.1 M $(NH_4)_2SO_4$; +10 V DC; several hours	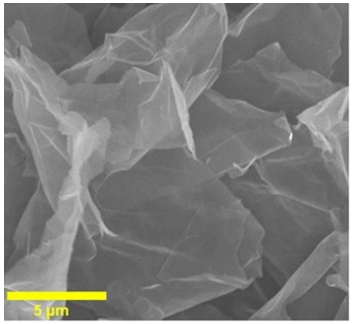 Wrinkled multilayer graphene sheets (<10 nm thick); C/O ratio = 4.98	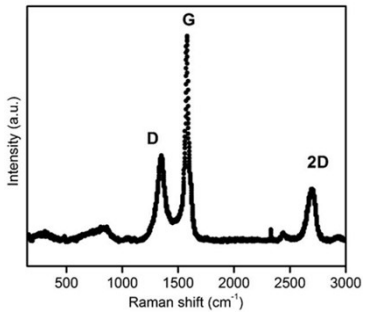 Laser source = 532 nm	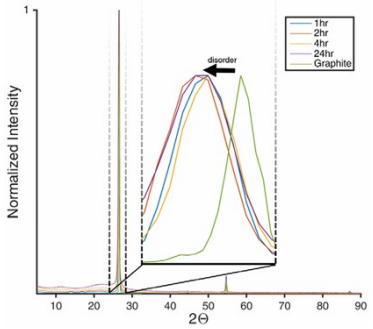 *Reproduced with permission from Ref. [25], Copyright 2018, Creative Commons Attribution 4.0*	25

0.1 M NaOH + Na_2SO_4; +10 V DC; complete exfoliation	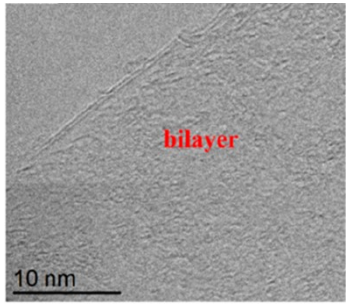 Multilayer graphene sheets (1-3 nm thick, 2-4 layers) C/O ratio = 19.1 (after thermal treatment)	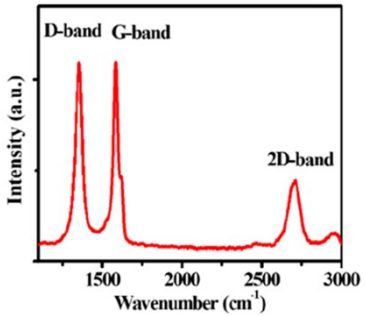 Laser source = 532 nm	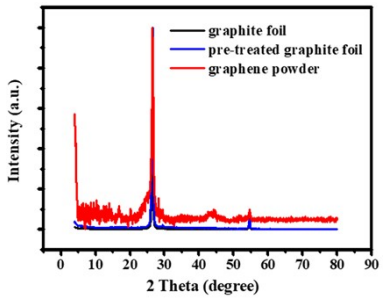 *Reproduced with permission from Ref. [26], Copyright 2019, American Chemical Society*	26
H_2SO_4; +5 V DC under ultra-sonication bath conditions; complete exfoliation (3 h)	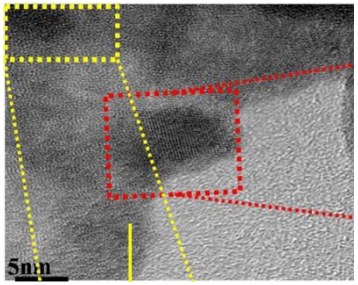 Multilayer graphene sheets (1-2 nm thick) C/O ratio = 3.74	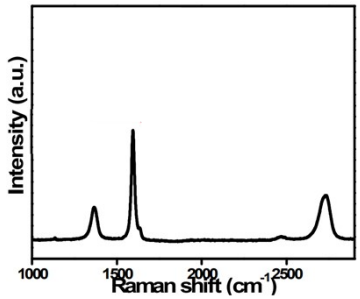 Laser source = 532 nm	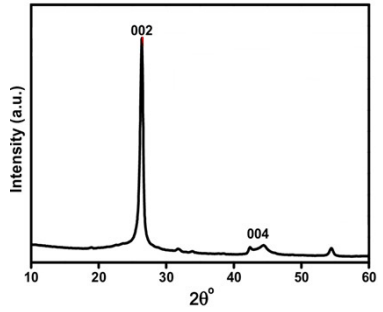 *Reproduced with permission from Ref. [27], Copyright 2012, The Royal Society of Chemistry*	27

tetra-n-butylammonium (TBA), ±5 V AC	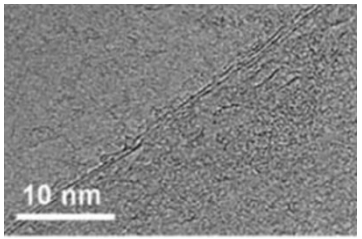 Multilayer graphene sheets (1-3 layers); C/O ratio = 17.2	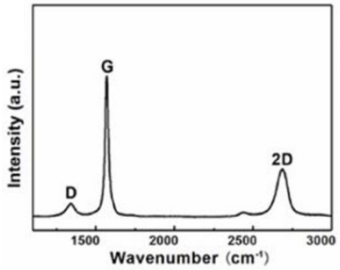 Laser source = 532 nm	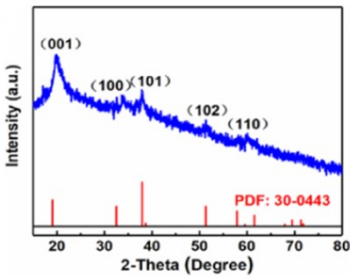 *Reproduced with permission from Ref. [28], Copyright 2018, Creative Commons Attribution 3.0 licence*	28

References

1 L. M. Malard, M. A. Pimenta, G. Dresselhaus and M. S. Dresselhaus, *Phys Rep*, 2009, 473, 51–87.

2 A. C. Ferrari and D. M. Basko, *Nat Nanotechnol*, 2013, 8, 235–246.

3 J. Bin Wu, M. L. Lin, X. Cong, H. N. Liu and P. H. Tan, *Chem Soc Rev*, 2018, 47, 1822–1873.

4 A. C. Ferrari and J. Robertson, *Phys Rev B*, 2000, 61, 14095–14107.

5 TUINSTRA F and KOENIG JL, *Journal of Chemical Physics*, 1970, 53, 1126–1130.

6 A. C. Ferrari and D. M. Basko, 2013, preprint, DOI: 10.1038/nnano.2013.46.

7 M. Lazzeri, C. Attaccalite, L. Wirtz and F. Mauri, *Phys Rev B*, 2008, 78, 081406.

8 D. M. Basko, S. Piscanec and A. C. Ferrari, *Phys Rev B*, DOI:10.1103/physrevb.80.165413.

9 I. Pocsik, M. Hundhausen, M. Koos and L. Ley, *Origin of the D peak in the Raman spectrum of microcrystalline graphite*, 1998, vol. 227.

10 C. Thomsen and S. Reich, *Phys Rev Lett*, 2000, 85, 5214–5217.

11 P. Venezuela, M. Lazzeri and F. Mauri, *Phys Rev B Condens Matter Mater Phys*, 2011, 84, 035433.

12 A. Sadezky, H. Muckenhuber, H. Grothe, R. Niessner and U. Pöschl, *Carbon N Y*, 2005, 43, 1731–1742.

13 D. Momodu, M. J. Madito, A. Singh, F. Sharif, K. Karan, M. Trifkovic, S. Bryant and E. P. L. Roberts, *Carbon N Y*, 2021, 171, 130–141.

14 M. J. Vujković, B. A. Vidoeski, S. P. Jovanović, D. V. Bajuk-Bogdanović, M. D. Budimir, Z. M. Marković, V. B. Pavlović, B. M. Todorović-Marković and I. D. Holclajtner-Antunović, *Electrochim Acta*, 2016, 217, 34–46.

15 F. Sharif, A. S. Zeraati, P. Ganjeh-anzabi, N. Yasri, S. M. Holmes, U. Sundararaj, M. Trifkovic and P. L. Roberts, *Carbon N Y*, 2020, 157, 681–692.

16 N. S. Mankge, D. Y. Momodu, N. W. Hlongwa, K. Makgopa, A. T. Kuvarega and M. J. Madito, *Synth Met*, 2024, 307, 117652.

17 K. Parvez, Z. S. Wu, R. Li, X. Liu, R. Graf, X. Feng and K. Müllen, *J Am Chem Soc*, 2014, 136, 6083–6091.

18 S. Yang, S. Brüller, Z. S. Wu, Z. Liu, K. Parvez, R. Dong, F. Richard, P. Samorì, X. Feng and K. Müllen, *J Am Chem Soc*, 2015, 137, 13927–13932.

19 S. Yang, A. G. Ricciardulli, S. Liu, R. Dong, M. R. Lohe, A. Becker, M. A. Squillaci, P. Samorì, K. Müllen and X. Feng, *Angewandte Chemie*, 2017, 56, 6669–6675.

20 C. H. Chen, S. W. Yang, M. C. Chuang, W. Y. Woon and C. Y. Su, *Nanoscale*, 2015, 7, 15362–15373.

21 T. N. J. I. Edison, R. Atchudan, N. Karthik, P. Chandrasekaran, S. Perumal, P. Arunachalam, P. B. Raja, M. G. Sethuraman and Y. R. Lee, *Surf Coat Technol*, 2021, 416, 127150.

22 L. Chao, Y. Qin, Y. Liu, Y. Kong and F. Chu, *Journal of Solid State Electrochemistry*, 2017, 21, 1287–1295.

23 J. M. Munuera, J. I. Paredes, S. Villar-Rodil, M. Ayán-Varela, A. Martínez-Alonso and J. M. D. Tascón, *Nanoscale*, 2016, 8, 2982–2998.

24 D. L. Vu, Y. J. Kwon, S. C. Lee, J. U. Lee and J. W. Lee, *Carbon Letters*, 2019, 29, 81–87.

25 T. C. Achee, W. Sun, J. T. Hope, S. G. Quitzau, C. B. Sweeney, S. A. Shah, T. Habib and M. J. Green, *Sci Rep*, 2018, 8, 1–8.

26 Z. Liu, H. Zhang, M. Eredia, H. Qiu, W. Baaziz, O. Ersen, A. Ciesielski, M. Bonn, H. I. Wang and P. Samorì, *ACS Nano*, 2019, 13, 9431–9441.

27 N. Parveen, M. O. Ansari, S. A. Ansari and M. H. Cho, *J Mater Chem A Mater*, 2016, 4, 233–240.

28 H. Shi, Y. Dong, F. Zhou, J. Chen and Z. S. Wu, *JPhys Energy*, DOI:10.1088/2515-7655/aadef6.